International Journal of GEOMATE, April., 2021, Vol.20, Issue 80, pp.76-81
ISSN: 2186-2982 (P), 2186-2990 (O), Japan, DOI: https://doi.org/10.21660/2021.80.GX223
Geotechnique, Construction Materials and Environment

COUPLED ANALYSIS CONSIDERING DENSITY CHANGE OF UNSATURATED SOIL

Daiki Yamashita [1] and *Shin-ichi Kanazawa [2]

[1] Social Environmental Systems Engineering Course, National Institute of Technology, Fukushima College, Advanced Course Program, Japan;
[2] Civil and Environmental Engineering, National Institute of Technology, Fukushima College, Japan

*Corresponding Author, Received: 15 Jun. 2020, Revised: 13 Jan. 2021, Accepted: 05 Feb. 2021

ABSTRACT: In recent years, with the increase in sudden heavy rainfall, such as typhoons and guerrilla heavy rain, there are many reports of the collapse of soil structures on a global scale. People are suffering from the danger of soil structure disasters almost every year. This is partly due to the analysis of the factors leading to the collapse of soil structures and the fact that the mechanisms are not fully understood. In this study, the ground behavior of embankment and river embankment considering rainfall and rising water level were examined using the air-dissolved unsaturated soil / water / air coupled finite analysis code. Therefore, in this study, in order to perform an analysis that takes into account the change in density, we proposed a new term "$\dot{\rho}$" in the incremental balance equation and attempted to examine it. In addition, analysis was performed under the same conditions as the analysis code that did not consider the density change, and the effectiveness of the density change consideration was confirmed.

Keywords : Numerical analysis, Density change, Unsaturated soil, Finite element method

1. INTRODUCTION

In recent years, due to the effects of global warming, sudden heavy rains such as typhoons and guerrilla heavy rains are increasing. Along with this, there are many reports of collapse of and damage to soil structures on a global scale. Even in Japan, due to the effects of Typhoon No. 19 in 2019, about 140 river dikes broke and suffered enormous damage nationwide [1]. At that time, many river dikes under the jurisdiction of the country, such as the YOSHIDA River (Miyagi), the ABUKUMA River (Fukushima), and the CHIKUMA River (Nagano), broke. This was partly due to the analysis of the factors leading to the collapse of soil structures and the fact that the mechanisms are not fully understood. Therefore, it is urgently necessary to understand the behavior of the foundation ground of soil structures over a long period of time. In geotechnical engineering, there are many studies looking at the optimal design of an embankment structure that focus on predicting the structure's long-term performance by using numerical analysis. In this laboratory, we have clarified the ground behavior of embankment and river embankment considering rainfall and rising water level using the air-dissolved unsaturated soil / water / air coupled finite analysis code "DACSAR-MP"[2]. However, in the current analysis code for unsaturated soil, the term of the density change over time in the incremental balancing equation is "$\dot{\boldsymbol{\sigma}} + \dot{\rho}\mathbf{g} = 0$" is "$\dot{\rho}\mathbf{g} = 0$". For this reason, the current analysis cannot consider state change due to external factors, that is, the influence of the density change of the unsaturated state. This is because the time change of the density "$\dot{\rho}$" is not formulated. Therefore, in this study, in order to perform an analysis that takes into account the change in density, we proposed a new term "$\dot{\rho}$" in the incremental balance equation and attempted to examine it. Therefore, the purpose of this research is to propose an analysis code considering the time change of the density by newly proposing the time change of the density and reflecting it in the DACSAR-MP program. In addition, we compare the analysis results with the conventional analysis code (without density change) and the newly constructed analysis code (with density change) to verify the usefulness of the change.

2. DENSITY CHANGE OVER TIME

2.1 Necessity

In conventional finite element analysis, it is not possible to consider the effect of state change due to external factors, that is, the effect of unsaturated density change. Taking the collapse of a river embankment as an example, overflow, erosion, seepage, and earthquakes are all causes of river embankment failure due to fluctuations in external water level. Of these, three, excluding earthquakes, are due to rainfall. Therefore, using the existing analysis code, we have tried to understand the behavior of soil structures by performing analysis with rainfall and water level rise for the river embankment. However, the existing analysis code cannot consider the effect of unsaturated density change. In other words, it is impossible to obtain more accurate analysis results because the density does not change with time, and it is not possible to consider the inflow and outflow of water into the ground. Therefore, it is necessary to propose the equilibrium formula of unsaturated soil for more precise analysis.

2.2 Proposal of a Term for Density Change with Time

First, Equation (1) shows the relationship of relative densities in each phase.

$$\bar{\rho}_\alpha = \frac{M_\alpha}{V} = \frac{V_\alpha}{V}\rho_\alpha (\alpha = s, f, a) \tag{1}$$

Here, the relative volume of each layer is expressed as follows from the relationship between the void ratio, porosity, and saturation and the three-phase diagram of soil. Equations (2), (3), and (4) are the relative volumes of the soil, liquid, and gas phases in this order.

$$\frac{V_s}{V} = \frac{1}{1+e} = \frac{n}{e} = \frac{n(1-n)}{n} = 1-n \tag{2}$$

$$S_r = \frac{V_w}{V_v} = \frac{\frac{V_w}{V}}{\frac{V_v}{V}} \Rightarrow \frac{V_w}{V} = S_r\frac{V_v}{V} = S_r\frac{V-V_s}{V} = nS_r \tag{3}$$

$$\frac{V_a}{V} = \frac{V-V_s-V_w}{V} = n(1-S_r) \tag{4}$$

From this, the relative density of each phase is as follows. Equations (5), (6), and (7) are the relative densities of the soil, liquid, and vapor phases in this order.

$$\bar{\rho}_s = (1-n)\rho_s \tag{5}$$

$$\bar{\rho}_w = nS_r\rho_w \tag{6}$$

$$\bar{\rho}_a = n(1-S_r)\rho_a \tag{7}$$

Therefore, Equation (8) shows the overall density relationship.

$$\rho = \bar{\rho}_s + \bar{\rho}_w + \bar{\rho}_a \tag{8}$$

Next, let us consider the time variation of the density of each phase. Equations (9), (10), and (11) are the changes over time in the density of the soil, liquid, and gas phases.

$$\dot{\bar{\rho}}_s = ((1-n)\rho_s)^{\bullet} = -\dot{n}\rho_s \tag{9}$$

$$\dot{\bar{\rho}}_w = (nS_r\rho_w)^{\bullet} = \dot{n}S_r\rho_w + n\dot{S}_r\rho_w \tag{10}$$

$$\dot{\bar{\rho}}_a = (n(1-S_r)\rho_a)^{\bullet} = \dot{n}(1-S_r)\rho_a - n\dot{S}_r\rho_a \tag{11}$$

Finally, the time variation of the overall density is expressed by Equation (12), so $\dot{\rho}$ is proposed as in Equation (13).

$$\dot{\rho} = \dot{\bar{\rho}}_s + \dot{\bar{\rho}}_w + \dot{\bar{\rho}}_a \tag{12}$$

$$\dot{\rho} = -\dot{n}\rho_s + \dot{n}S_r\rho_w + n\dot{S}_r\rho_w + \dot{n}(1-S_r)\rho_a - n\dot{S}_r\rho_a \tag{13}$$

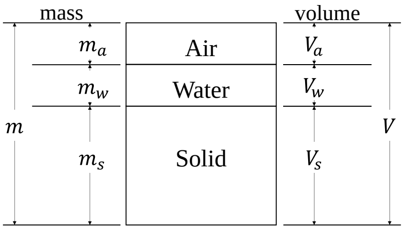

Fig. 1 Three-phase diagram of soil

2.3 Density Change Reflected In the Analysis Code

For the effective stress equation considering the term of density change with time, which was proposed in the previous section, weak formulation was performed. After that, spatial discretization was performed using the finite element method. Furthermore, time discretization was performed by the Euler method. This formula, reflected in the program of the analysis code "DACSAR-MP"[2] (see the next chapter), is used in this laboratory, and a new analysis code was created in consideration of the effect of temporal density changes.

3. SOIL/WATER/AIR COUPLED FINITE ANALYSIS CODE

The finite element analysis code “DACSAR-MP” [2] used in this study formulates the unsaturated soil constitutive model proposed by Ohno, Kawai and Tachibana [3]. This model is framed as the soil/water/air coupled problem using the three-phase mixture theory. Equation (14) shows the effective stress. Equation (15) shows the base stress tensor and suction stress. Equation (16) shows suction.

$$\boldsymbol{\sigma}' = \boldsymbol{\sigma}^{\mathbf{net}} + p_s \mathbf{1} \tag{14}$$

$$\boldsymbol{\sigma}^{\mathbf{net}} = \boldsymbol{\sigma} - p_a \mathbf{1} \;\;,\;\; p_s = S_e s \tag{15}$$

$$s = p_a - p_w \;\;,\;\; S_e = \frac{S_r - S_{rc}}{1 - S_{rc}} \tag{16}$$

Here, $\boldsymbol{\sigma}'$ is the effective stress tensor; $\boldsymbol{\sigma}^{\mathbf{net}}$ is the base stress tensor; $\mathbf{1}$ is the second order unit tensor; $\boldsymbol{\sigma}$ is the total stress tensor; s is the suction; p_s is the suction stress; p_a is the pore air pressure; p_w is the pore water pressure; S_r is the degree of saturation; S_e is the effective degree of saturation; and S_{rc} is the degree of saturation at s→∞. In numerical calculations, the EC model of Ohno, Iizuka and Ohta [4], which does not have a singularity in the yield surface, was incorporated to avoid shifting to the singularity, a quantity impossible to differentiate, during preconsolidation pressure at saturation. Equations (17), (18), (19) and (20) provide the yield function.

$$f\left(\boldsymbol{\sigma}', \zeta, \varepsilon_v^p\right) = MD \ln \frac{p'}{\zeta p'_{sat}} + \frac{MD}{n_E}\left(\frac{q}{Mp'}\right)^{n_E} - \varepsilon_v^p = 0 \tag{17}$$

$$\xi = \exp\left[(1 - S_e)^{n_s} \ln a\right] \;\;,\;\; MD = \frac{\lambda - \kappa}{1 + e_0} \tag{18}$$

$$p' = \frac{1}{3} \boldsymbol{\sigma}' : \mathbf{1} \;\;,\;\; q = \sqrt{\frac{3}{2} \mathbf{s} : \mathbf{s}} \tag{19}$$

$$\mathbf{s} = \boldsymbol{\sigma}' - p' \mathbf{1} = \mathbf{A} : \boldsymbol{\sigma}' \;\;,\;\; \mathbf{A} = \mathbf{I} - \frac{1}{3} \mathbf{1} \otimes \mathbf{1} \tag{20}$$

Here, n_E is the shape parameter; ε_v^p is the plastic volume strain; M is the *q/p'* in the limit state; D is the dilatancy coefficient; p_{sat} is the yield stress at saturation; a and n_s are the parameters representing the increase in yield stress due to unsaturation; λ is the compression index; and κ is the expansion index. Equation (21) shows pore water velocity. Equation (22) shows air velocity. Pore water and air flow follow Darcy's law.

$$\tilde{v}_w = -\mathbf{k_w} \cdot \mathrm{grad} h \tag{21}$$

$$\tilde{v}_a = -\mathbf{k_a} \cdot \mathrm{grad} h_a \;\;,\;\; h_a = \frac{p_a}{\gamma_w} \tag{22}$$

Here, $\tilde{v}_w$ is the pore water velocity; $\tilde{v}_a$ is the air velocity; $\mathbf{k_w}$ is the hydraulic conductivity; $\mathbf{k_a}$ is the coefficient of air permeability; h is the total head; γ_w is the unit weight of water; and h_a is the pneumatic head. Equations (23)-(24) show hydraulic conductivity and the coefficient of air permeability by way of Mualem's [5] formula and the Van Genuchten [6] formula.

$$\mathbf{k_w} = k_{rw} \mathbf{k_{wsat}} = S_e^{1/2}\left[1 - \left(1 - S_e^{1/m}\right)^m\right]^2 \mathbf{k_{wsat}} \tag{23}$$

$$\mathbf{k_a} = k_{ra} \mathbf{k_{ares}} = \left(1 - S_e\right)^{1/2}\left(1 - S_e^{1/m}\right)^{2m} \mathbf{k_{ares}} \tag{24}$$

Here, k_{rw} is the ratio of hydraulic conductivity; k_{ra} is the ratio of coefficient of air permeability; m is the Mualem constant; $\mathbf{k_{wsat}}$ is the hydraulic conductivity at saturation; $\mathbf{k_{ares}}$ is the coefficient of air permeability in dry conditions. Equations (25)-(26) show the continuous formula of pore water and air using three-phase mixture theory.

$$n\dot{S}_r - S_r \dot{\varepsilon}_v + \mathrm{div} \tilde{v}_w = 0 \tag{25}$$

$$(1 - S_r)\dot{\varepsilon}_v + n\dot{S}_r - n(1 - S_r)\frac{\dot{p}_a}{p_a + p_0} - \mathrm{div} \tilde{v}_a = 0 \tag{26}$$

Here, n is porosity; $\dot{\varepsilon}_v$ is volumetric strain; and p_0 is atmospheric pressure. The elasto-plastic constitutive model obtained from Equation (17) and the equilibrium equation [Equations (25) - (26)] are formulated as the soil/water/air coupled problem.

4. COMPARATIVE ANALYSIS

In this study, we examined the validity of the newly proposed analysis code that includes the effect of temporal density changes. Analyses were performed using the conventional analysis code that does not consider the influence of temporal density change (hereinafter, old analysis code) and the analysis code proposed here that considers the influence of temporal density change (hereinafter, new analysis code). The two analysis codes were used under the same analytical conditions, and a comparative study was conducted.

4.1 Analysis Condition

The new and old analysis codes for the soil / water / air coupled finite code "DACSAR-MP" [2] were used under the same conditions.

4.1.1 Moisture characteristic curve used by analysis

For a soil-water characteristic curve model, a model capable of hysteresis expression, as proposed by Kawai, Wang and Iizuka [7], is used. In addition, to determine the logistic curve in the case of DRY and WET, derived from arbitrary suction and the degree of saturation, the logistic curve equation of Sugii and Uno [8] was used. This makes it possible to grasp the moisture conditions of sloped ground where a complex water balance occurs. Figure 2 shows the soil-water characteristic curve used in this study.

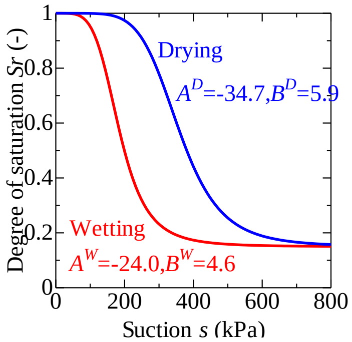

Fig.2 Soil water characteristic curve

4.1.2 Material parameters

Table 1 shows the material parameters used in this study. Material parameters were determined considering the results of previous studies by Honda, Iizuka, Ohno, Kawai and Wang [9]. Here, λ is the compression index; κ is the swelling index; M is the marginal state parameters; m is the unsaturated permeability coefficient of Mualem; n is the E_c model parameters; n_E is the magnification ratio of yield surface; e_0 is the initial gap ratio; ν is the Poisson's ratio; and S_{r0} is the critical degree of saturation. In this analysis, the sand-mixed silt used for general soil structures is assumed.

Table 1 Material parameters

λ	κ	M	m	n
0.180	0.037	1.33	0.80	1.0
n_E	e_0	ν	S_{r0}	G_S
1.3	1.2	0.33	0.15	2.7
k_x [m/day]	k_y [m/day]	ρ_a [t/m^3]		
0.10	0.10	0.0012		

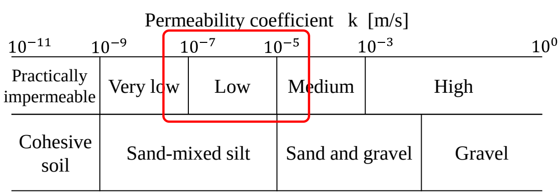

Fig. 3 Permeability coefficient

4.1.3 Analysis model

Figure 4 shows the analytical model used for the comparative analysis. The numbers in the figure indicate element numbers. The displacement boundaries are as follows.

Upper side : Free
Bottom : x, y axis fixed
Right side : x-axis fixed
Left side : x-axis fixed

Here, the water head boundary is given an undrained condition. The air boundary is a non-exhaust condition.

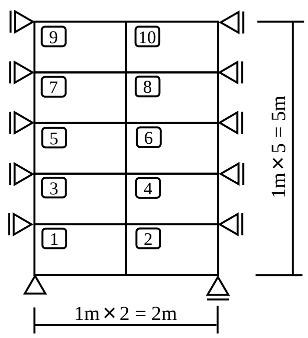

Fig. 4 Analysis model

4.1.4 Flow condition

As the flow rate condition in this analysis, 1.0×10^{-3}m/day rainfall was applied to the upper surface of the model for 900 days (90000 steps). At this time, the daily average rainfall of 5.0×10^{-3}m/day was calculated from the annual average rainfall of 1529mm/year in Tokyo [10], and the rainfall was set so that it did not differ much from the actual rainfall. The initial saturation was $S_r = 60\%$.

4.2 Analysis Result

In this study, we compare the analysis results of the new and old analysis codes regarding saturation, volume strain and total stress. In addition, for the new analysis code, we verified the reaction force at the bottom of the model.

4.2.1 Change in Saturation (S_r)

Figure 5 shows the degree of saturation values and the differences in the analysis using the new and old analysis codes at typical STEP numbers. (The difference is the result of the new analysis code minus the result of the old analysis code.)

From Figure. 5, we can confirm the difference in the degree of saturation in the analysis using the new and old analysis codes. Here, both results show a similar degree of saturation increase as the number of STEPs increase. Furthermore, the evaluation is performed by focusing on the number of steps. First, from the time immediately after the analysis to the early stage of analysis, the results from the old analysis code show a slightly higher degree of saturation, but the difference is only 0.0095% at the time of STEP10000. In other words, from the time immediately after the analysis to the beginning, there is almost no effect due to the consideration of $\dot{\rho}$ in the incremental balance equation. However, as the number of STEPs increases, the difference in degree of saturation increases rapidly. Figure 6 shows the difference in degree of saturation between the new and old analysis codes. As shown here, the difference in saturation exhibits an exponential relationship. For this reason, the difference in degree of saturation in this analysis becomes noticeable at around STEP 40000. Furthermore, it is clear that at STEP80000, the difference becomes a remarkable discrepancy of about 2.1%.

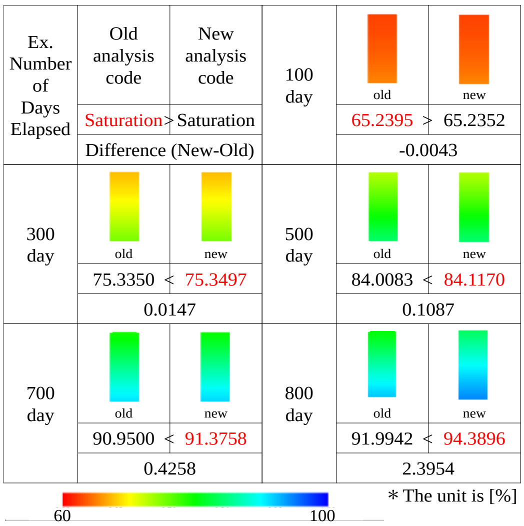

Fig. 5 Change in degree of saturation

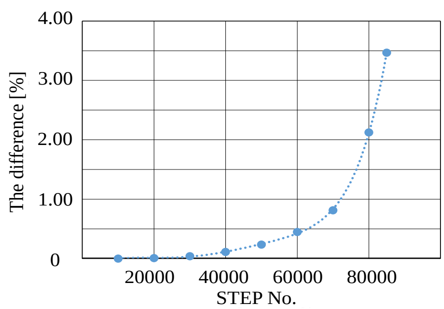

Fig. 6 Difference in saturation between new and old analysis codes

4.2.2 Total stress

The changes over time of total stress in the analysis using the new and old analysis codes are shown below. Figure 7 shows the upper model, and Figure 8 shows the lower model. As seen in Figures 7 and 8, the total stress value in the new analysis code exceeds the total stress value in the old analysis code in both the upper and lower parts of the model. This is the effect of the consideration of $\dot{\rho}$ on the incremental balance formula. It is considered that the newly proposed ρ term affects the distribution of total stress immediately after the analysis. This suggests that the density term has a large effect on the total stress.

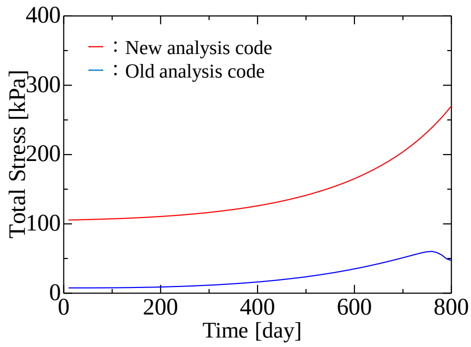

Fig.7 Total stress at the top of the model

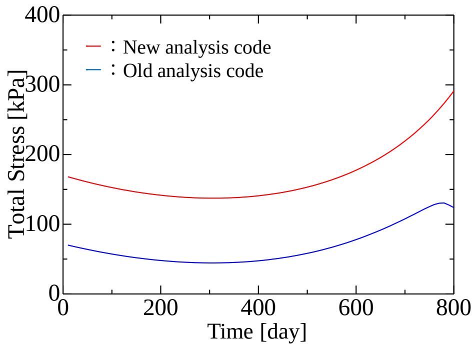

Fig.8 Total stress at the bottom of the model

4.2.3 Reaction force verification

In this study, we also verified the reaction force to confirm the consistency of the new analysis code considering the time variation of density. Figure 9 is a model that measures the reaction force. The model is a 1m x 1m element with nine nodes. The displacement boundaries are as follows.

Upper side : Free
Bottom : x, y axis fixed
Right side : x-axis fixed
Left side : x-axis fixed

In addition, the water head boundary is an undrained condition and the air boundary is a non-exhaust condition. As the flow rate condition, 10 days (1000 steps) of 1.0×10^{-2} m/day rainfall was applied to the top of the model. Table 2 summarizes the results. Table 2 shows the reaction force values at the main STEPs at the contact points at the bottom of the model, "No. 1, No. 2, No. 3" and their totals. As a result, the reaction force at the bottom of the model increases as the number of steps increases. This confirms that the new analysis code is properly processing the flow rate condition, and the analytical consistency is therefore recognized.

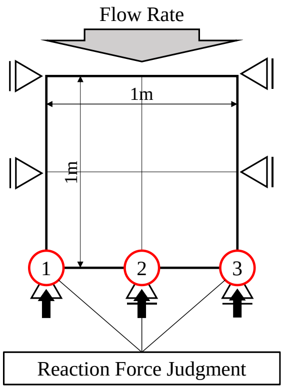

Fig.9 Reaction force verification model

Table 2 Total stress value

	No.1	No.2	No.3	Total
250	1.128	3.963	0.657	5.749
500	1.364	4.719	1.020	7.102
750	1.638	5.562	1.452	8.652
1000	1.933	6.377	1.923	10.232

* Positive Upward $\times 10^{-2}$ [kN]

5. CONCLUSIONS

First, the reaction force verification confirmed the consistency of the new analysis code. The analysis results using the new analysis code also confirmed that saturation and total stress tended to increase compared to the old analysis code. This demonstrated that the influence of the temporal change of density in the incremental balance equation cannot be ignored in the numerical analysis of unsaturated soil. It became particularly clear that the difference in the degree of saturation increases with the increase in the number of STEPs, suggesting that the difference becomes large in long-term analysis. Furthermore, in this study, analysis was performed considering the average flow rate in Japan. However, the change in the degree of saturation becomes more remarkable when the analysis considers a flow rate that corresponds to the sudden heavy rain which has frequently occurred in recent years. In other words, this strongly suggests that the effect of the change in density over time cannot be ignored. Moreover, many of the numerical analyses in geotechnical engineering aim at long-term prediction. Therefore, in long-term analysis, such as embankment analysis, a large difference between the results of the old analysis code and the new analysis code are expected. In the future, we will perform more detailed analysis, in addition to changing external factors, to confirm embankment behavior more precisely.

6. REFERENCES

[1] Cabinet Office: About the damage situation to affect typhoon 19th in the first year of Reiwa, pp24-25, 2020.

[2] Kanazawa S., Toyoshima K., Kawai K., Tachibana S. and Iizuka A.: Analysis of mechanical behavior of compacted soil with F.E. method, journal of JSCE, No.68 (2), pp.291-298, 2012.

[3] Ohno S., Kawai K. and Tachibana S.: Elastoplastic constitutive model for unsaturated soil applied effective degree of saturation as a parameter expressing stiffness, Journal of JSCE, Vol.63/No.4, pp.1132-1141, 2007.

[4] Ohno S., Iizuka A. and Ohta H., Two categories of new constitutive derived from non-linear description of soil contractancy, Journal of JSCE, Vol.9, pp.407-414, 2006.

[5] Mualem Y.: A new model for predicting the hydraulic conductivity of unsaturated porous media, Water Re-sources Research, Vol.12, No.3, pp.514-522, 1976.

[6] Van Genuchten: A closed-form equation for predicting hydraulic of unsaturated soils, Soil Science Society American Journal, Vol.44, pp.892-898, 1980.

[7] Kawai K., Wang W. and Iizuka A.: The expression of hysteresis appearing on water characteristic curves and the change of stresses in unsaturated soils, Journal of applied mechanics, Vol.5, pp.777-784, 2002.

[8] Sugii T. and Uno T.: Modeling the New Moisture Characteristic Curve, Journal of JSCE, pp.130-131, 1995.

[9] Honda M., Iizuka A., Ohno S. Kawai K. and Wang W.: A study of the evaluation method for deformation characteristic of compacted soil, Journal of JSCE, Vol.40, No.2, pp.99-110, 2000.

[10] Ministry of Internal Affairs and Communications Statistics Bureau: Japanese statistics 2019, p6, 2019.